

Search for periodic gravitational radiation with the ALLEGRO gravitational wave detector

E. Mauceli*, M. P. McHugh, W. O. Hamilton, W. W. Johnson, and A. Morse
Department of Physics and Astronomy, Louisiana State University, Baton Rouge, LA 70803, USA
(November 5, 2018)

We describe the search for a continuous signal of gravitational radiation from a rotating neutron star in the data taken by the ALLEGRO gravitational wave detector in early 1994. Since ALLEGRO is sensitive at frequencies near 1 kHz, only neutron stars with spin periods near 2 ms are potential sources. There are no known sources of this type for ALLEGRO, so we directed the search towards both the galactic center and the globular cluster 47 Tucanae. The analysis puts a constraint of roughly 8×10^{-24} at frequencies near 1 kHz on the gravitational strain emitted from pulsar spin-down in either 47 Tucanae or the galactic center.

04.80.Nn

I. INTRODUCTION

The majority of experimental searches for gravitational radiation have focused on the detection of burst signals, such as those emitted from the collapse of a massive star. There are compelling arguments that nearby millisecond pulsars can provide a detectable source of continuous (CW) gravity waves [1]- [2]. We will use the term “pulsar” in the following text to refer to a rotating neutron star, regardless of whether it is emitting detectable electromagnetic radiation.

It is well known that a symmetric object rotating about its symmetry axis does not emit gravitational radiation. Therefore, if a pulsar is to radiate gravity waves, it must either be asymmetric or precessing. For the purposes of this search, we have considered only asymmetric pulsars. The asymmetry can be rotationally induced or due to a “star quake” deforming the neutron star crust or due to some other process. By any mechanism, the amount of ellipticity produced in the neutron star is expected to be small, from a maximum of 10^{-5} , which, for some pulsar models is the maximum supportable asymmetry of the neutron star crust [3] to less than 10^{-9} . The latter number is obtained by assuming the measured spin-down of certain millisecond pulsars is due entirely to the emission of gravitational radiation.

In this article we report the results of our first search for a CW signal in data taken by the ALLEGRO resonant gravitational wave detector at Louisiana State University during the first three months of 1994 [4]. Another search has been performed by the EXPLORER detector team from the University of Rome, which has a similar detector and is pursuing a different type of analysis [5].

If there were known pulsars with the right spin period, they would be the natural target for any CW search. But there are only a small number of known pulsars with spin periods small enough (2.2 milliseconds) to match our antenna’s 900 Hz frequency and none of those listed in the 1995 Taylor pulsar catalog [6] has a spin period that matches our two narrow reception bands. We would ideally like to make an all sky search, but this is computationally very intensive. Given limited computing resources it is nearly impossible to exhaust all of the obvious possibilities. All-sky search strategies have been proposed elsewhere [7].

Therefore we have chosen another strategy and directed our first search towards two regions where one might reasonably expect to find a high density of CW sources. The first is the globular cluster 47 Tucanae (Tuc), and the second is the center of the galaxy. The celestial coordinates for both are listed in Table I. We chose 47 Tuc because it is relatively close, and because of the large number of fast millisecond pulsars known to be concentrated in this globular cluster [8], which suggests the possibility of more undetected neutron stars with short spin periods.

The analysis assumes the simplest possible CW source, one that has a stable emission frequency in its rest frame. In other words it is not spinning down and has no companions to cause orbital doppler shifts. In this case only knowledge of the earth’s motion and the antenna’s reception pattern are needed to determine the modulation of the frequency and amplitude of the received signal. These modulations are highly dependent on the source location. At the frequency resolution of our search, if the actual source location is offset from the supposed location by as

*Present address: Center for High Energy Physics, University of Oregon, Eugene, OR, 97403, USA

little as $1.00'$ in right ascension and $0.25'$ in declination, the gravitational wave frequency will be mis-identified by 1 bin [9]. However, the range of possible locations for detection of the signal (albeit with the frequency mis-identified) is significantly larger [10].

II. ALLEGRO

The ALLEGRO gravitational wave detector [4] is located in the Physics Building at Louisiana State University in Baton Rouge, Louisiana ($30^\circ.413$ N lat, $91^\circ.179$ W long). ALLEGRO consists of a resonant aluminum bar equipped with a resonant inductive transducer and a dc SQUID amplifier all cooled to 4.2 K. The bar is 60 cm in diameter and 300 cm in length, with a physical mass of 2296 kg. The bar is oriented perpendicular to the plane of the great circle on the Earth that passes through Geneva, the location of the Rome Explorer antenna, and midway between Baton Rouge, LA and Stanford, CA. This orientation results in the axis of ALLEGRO being directed along a line $40^\circ.4$ west of North.

Vibrations of our resonant antenna produce a voltage out of the SQUID electronics which is proportional to the relative displacement of the bar and transducer. The coupled system of bar and transducer has two normal modes at roughly 896.8 Hz and 920.3 Hz. These are referred to as the “minus” and “plus” resonant modes respectively. ALLEGRO is most sensitive in a small bandwidth around each of these modes. The voltage out of the SQUID electronics is sent to a single lock-in detector which demodulates and low pass filters the signal. The reference frequency of the lock-in is set halfway between the normal mode frequencies of the antenna, thus shifting the frequency of the signal from near 1 kHz to near 10 Hz. The output consists of in-phase (x) and quadrature (y) components which contain the full amplitude and phase information. The demodulated data is then sampled 125 times a second and written to disk.

III. TARGET SOURCE

We describe the gravity wave in a reference frame which has its $\hat{e}_{z'}$ axis aligned with the direction of propagation of the wave. This frame is referred to as the “wave frame” and is denoted by primed coordinates (x', y', z'). The most general form of the gravity wave in the wave frame is

$$\mathbf{h}_{wave} = \begin{bmatrix} h_+(t') & h_\times(t') & 0 \\ h_\times(t') & -h_+(t') & 0 \\ 0 & 0 & 0 \end{bmatrix} \quad (1)$$

where $h_+(t')$ and $h_\times(t')$ are the amplitudes of the two allowed states of linear polarization, referred to as the plus and cross amplitudes respectively.

In General Relativity one can compute the polarization amplitudes for a rotating, asymmetric neutron star using the quadrupole approximation [11]. We choose for our model a neutron star with the three principle moments of inertia about the three principle axes fixed in the body frame, denoted by I_1, I_2 and I_3 . The rotation axis is chosen to be along I_3 and the neutron star is assumed to be deformed such that $I_1 \neq I_2$. The ellipticity of the pulsar is then defined to be

$$\epsilon = \frac{I_1 - I_2}{I_3}. \quad (2)$$

The resulting gravitational radiation is emitted at twice the pulsar rotation frequency and the two polarization amplitudes are given by

$$\begin{aligned} h_+(t') &= h_c (1 + \cos^2 i) \cos(2\pi f_0 t') \\ h_\times(t') &= 2 h_c \cos i \sin(2\pi f_0 t') \end{aligned} \quad (3)$$

where the angle i is measured between the pulsar spin axis and the line of sight to the detector, h_c is the “characteristic amplitude” [1] of the incident wave, and $f_0 = 2f_{rot}$ is the frequency of the gravitational wave, equal to twice the rotation frequency of the pulsar. This is not the most general pulsar model one could construct. If the neutron star deformation is not along a principle axis, then emission occurs at the rotation frequency and twice the rotation frequency [12]. If the star is precessing, emission occurs at the rotation frequency, and the rotation frequency plus or minus the precession frequency [13]. For this work, we consider only emission at twice the rotation frequency.

The characteristic amplitude¹ is given by

$$h_c = \frac{2G}{c^4 r} \epsilon I_3 (\pi f_0)^2 \quad (4)$$

where r is the distance to the source, G is the gravitational constant, and c the speed of light. Adopting a value of $I_3 = 10^{45} \text{ g cm}^2$ (a reasonable estimate for a $1.4M_\odot$ pulsar with a radius of 10 km), this can be written as

$$h_c = 5.2 \times 10^{-28} \left(\frac{I_3}{10^{45} \text{ g cm}^2} \right) \left(\frac{\epsilon}{10^{-8}} \right) \left(\frac{10 \text{ kpc}}{r} \right) \left(\frac{f_0}{1 \text{ kHz}} \right)^2. \quad (5)$$

For galactic sources ($< 10 \text{ kpc}$), and assuming the maximum allowed pulsar ellipticity ($\epsilon \sim 10^{-5}$) we see that the characteristic amplitude is of order 10^{-24} . As will be shown, this is of the same level as the measurements.

IV. PHASE CONSIDERATIONS

Reliable detection of a periodic gravitational wave signal depends on tracking the phase of the signal through many cycles. As given in Eq. 3, the polarization amplitudes of the gravity wave are pure sinusoids at an unknown frequency. Detection of such a signal would involve a single Fourier transform of the data, the resulting spectrum then being scanned for anomalous peaks. However, the phase of the gravity wave as observed at the detector at a particular observation time, relative to the emitted phase, depends on a number of factors: 1) intrinsic pulsar spin-down, 2) motion of the Earth within the solar system, 3) if it is part of a binary system, orbital motion of the pulsar, and 4) proper motion of the pulsar. This results in the initially narrow-band signal being spread out over many frequency bins, decreasing the signal to noise ratio of the single Fourier transform. As the expected signals are already weak, this seriously compromises one's detection capabilities. For the purposes of this work, we assume that the pulsar is solitary with negligible spin-down, and has no other accelerations with respect to the solar system barycenter (SSB). We also assume the proper motion of the pulsar is small such that it does not move significantly during the observation time.

It should be noted that the spindown due to the emission of gravitational radiation at the level of sensitivity of this experiment would be quite significant. The lack of an actual target source has led us to choose the simplest case for the purposes of demonstration of the potential sensitivity of a real detector. With these assumptions, the phase of the carrier frequency is modulated only by motion of the Earth in the solar system, with the modulation being given by (see Fig. 1)

$$\Phi(t) = \omega_0 \left(\frac{1}{c} \mathbf{r}(t) \cdot \hat{\mathbf{n}} + 1.658^{ms} \sin g(t) \right) \quad (6)$$

where $\mathbf{r}(t)$ is the vector from the SSB to the center of mass of the detector at observation time t , $\hat{\mathbf{n}}$ is a unit vector from the SSB directed towards the pulsar, c is the speed of light, and $\omega_0 = 2\pi f_0$. The second term is due to the combined effect of time dilation and gravitational redshift due to the solar system bodies. It is periodic over a year with maximum delay of 1.7 ms. We note that the angle $g(t)$ varies slightly from year to year. In 1994 its value was

$$g(t)/2\pi = 356.60 + 0.98560 \times D$$

where D is the day of the year. Including this information into Eq. 3, we write the two polarizations of the gravity wave as (expressed in a frame parallel to the wave frame)

$$\begin{aligned} h_+(t) &= h_c (1 + \cos^2 i) \cos(\omega_0 t + \Phi(t) + \Phi_0) \\ h_\times(t) &= h_c (2 \cos i) \sin(\omega_0 t + \Phi(t) + \Phi_0) \end{aligned} \quad (7)$$

where Φ_0 is an unknown, constant offset.

Astronomical locations are usually given as right ascension and declination coordinates, denoted α, δ respectively. These are defined in the the ‘‘celestial’’ coordinate frame (CC frame with coordinates (X, Y, Z)). This frame is centered

¹New's characteristic strain is greater by a factor of 2 as they assumed that the rotation axis of the pulsar was along the line of sight to the Earth.

at the solar system barycenter (SSB) with \hat{e}_Z along the Earth's rotation axis. \hat{e}_X and \hat{e}_Y are in the Earth's equatorial plane with \hat{e}_X directed towards the intersection of the equatorial plane with the Earth's orbital plane (the ecliptic) at the vernal equinox. Right ascension is measured in hours of angle (12 hrs = π radians) from the vernal equinox eastward along the celestial equator to the celestial object and declination is measured in degrees north (+) or south (-) of the equatorial plane.

To calculate the dot product in the phase modulation term, we also expressed the detector position in the CC frame. This was done in two steps. First, the position of the center of mass of the Earth relative to the SSB was obtained using a commercially available software package from the U.S. Naval Observatory (MICA²). MICA uses the Jet Propulsion Laboratory DE200/LE200 ephemeris. It reports positions of the Earth's center of mass in a cartesian coordinate frame centered at the SSB. Coordinates are given to the nearest 10^{-9} astronomical units (AU), which is of order 10^2 meters. This corresponds to 1/1000 of a wavelength for the signals of interest here, enabling an accurate tracking of the phase of the gravitational wave.

Second, a GPS receiver was used to obtain the latitude and longitude coordinates of ALLEGRO, again with sufficient accuracy to track the signal. These were converted to cartesian coordinates in a frame centered at the Earth's center of mass and vectorally added to the center of mass positions to provide ALLEGRO's position with respect to the SSB. The cartesian coordinates for ALLEGRO were converted to the spherical coordinates (r, t_s, δ_A) : r being the distance from the SSB to the detector, t_s the local sidereal time, and δ_A the declination of the detector. Using the spherical trigonometric formula for the cosine of the angle between two vectors, we write the phase delay as

$$\Phi(t) = 2\pi f_0 \left(\frac{r(t)}{c} [\sin \delta_A \sin \delta + \cos \delta_A \cos \delta \cos \gamma(t)] + 1.658^{ms} \sin g(t) \right) \quad (8)$$

where $\gamma = t_s - \alpha$ is the local hour angle.

V. SIGNAL CONSIDERATIONS

A passing gravity wave provides the largest fractional change in the length of a bar, and therefore the largest signal in a bar detector, when its direction of propagation is perpendicular to the bar axis and one of the polarizations of the gravity wave lies along the bar axis. In general, the gravity wave is incident to the bar with some arbitrary angle and polarization. We define the polarization angle as the angle between the bar axis (west of North) and the direction of the plus polarization of the gravity wave.

We describe the detector in a coordinate frame whose origin is at the center of mass of the antenna, with the \hat{e}_z axis aligned with the local vertical and the \hat{e}_x axis aligned with the bar axis. This frame is referred to as the "lab frame" and is denoted denoted by unprimed coordinates (x, y, z) .

For a gravity wave incident with an arbitrary orientation to the bar axis, it is only the component of the strain tensor along the bar axis which produces a detectable driving force on the bar. This force is commonly written as

$$\mathcal{F}(t) = \frac{1}{2} \mu L_e \ddot{h}_{xx}(t) \quad (9)$$

where $\ddot{h}_{xx}(t)$ is the second time derivative of the strain component along the bar axis. The quantities μ and L_e are the effective mass and length of the first longitudinal eigenmode of the bar, obtained by solving the elastic equations of motion for a long, thin cylinder. The effective mass is equal to half the physical mass of the bar ($\mu = 1148$ kg) and $L_e = (4/\pi^2)L$ where $L=3$ m is the actual length of the bar. The force acting on the bar dominates the output as the force on the transducer itself produces a much smaller motion.

To calculate the component of the gravitational wave, given by Eq. 1 in the wave frame, along the bar axis requires knowledge of the rotation matrix between the wave frame and the lab frame. As both source direction and detector locations are known, the rotation matrix is completely specified (up to an angle related to the unknown polarization of the gravity wave). We calculate the rotation matrix by first rotating the wave frame to the CC frame, and then the CC frame to the lab frame. The full rotation matrix from the wave frame to the lab frame is given by

$$\mathbf{R}_{wave \rightarrow lab} = \mathbf{R}_{CC \rightarrow lab} \mathbf{R}_{wave \rightarrow CC} \quad (10)$$

²Multiyear Interactive Computer Almanac, U.S. Naval Observatory, 3450 Mass. Ave., N.W. Washington, DC 20392

The CC frame is related to the wave frame by the angles ($\phi = \alpha - \pi/2, \theta = \delta + \pi/2, \psi = \psi_0$), where we have used the Euler x-convention to define the axes of rotation. Using Eq. 4-46 of Goldstein [14], with the stated angular substitutions, the rotation matrix from the wave frame to the CC frame is given by

$$\mathbf{R}_{wave \rightarrow CC} = \begin{pmatrix} (\sin \alpha \cos \psi_0 - \cos \alpha \sin \delta \sin \psi_0) & (-\sin \psi_0 \sin \alpha - \cos \psi_0 \cos \alpha \sin \delta) & (-\cos \alpha \cos \delta) \\ (-\cos \psi_0 \cos \alpha - \sin \psi_0 \sin \alpha \sin \delta) & (\sin \psi_0 \cos \alpha - \cos \psi_0 \sin \alpha \sin \delta) & (-\sin \alpha \cos \delta) \\ (\sin \psi_0 \cos \delta) & (\cos \psi_0 \cos \delta) & (-\sin \delta) \end{pmatrix}.$$

Again using the x-convention to define the rotation axes, the CC frame is related to the laboratory frame by the angles ($\phi = t_s + \pi/2, \theta = \pi/2 - l, \psi = \pi/2 + \eta$). t_s is the detector local sidereal time as before and l is the detector latitude. The particular value for the final rotation angle comes from the choice to define the \hat{e}_x axis pointing west of North along the bar axis. The rotation matrix from CC frame to lab frame is then

$$\mathbf{R}_{CC \rightarrow lab} = \begin{pmatrix} (\sin \eta \sin t_s - \sin l \cos t_s \cos \eta) & (-\sin \eta \cos t_s - \sin l \sin t_s \cos \eta) & (\cos \eta \cos l) \\ (\cos \eta \sin t_s + \sin l \cos t_s \sin \eta) & (-\cos \eta \cos t_s + \sin l \sin t_s \sin \eta) & (-\sin \eta \cos l) \\ (\cos l \cos t_s) & (\cos l \sin t_s) & (\sin l) \end{pmatrix}.$$

Using Eq. 10, the full rotation matrix may be computed and h_{xx} is the (11) component of

$$\mathbf{h}_{lab} = \mathbf{R}_{wave \rightarrow lab} \mathbf{h}_{wave} \mathbf{R}_{wave \rightarrow lab}^T. \quad (11)$$

Considering only the component of the gravity wave along the bar axis,

$$h_{bar}(t) = (R_{11}^2 - R_{12}^2) h_+(t) + 2 R_{11} R_{12} h_\times(t)$$

where the relevant components of the rotation matrix are

$$\begin{aligned} R_{11} &= \cos \psi_0 (\sin \eta \cos \gamma + \sin l \cos \eta \sin \gamma) \\ &\quad + \sin \psi_0 (-\sin \eta \sin \delta \sin \gamma + \sin l \cos \eta \sin \delta \cos \gamma + \cos \eta \cos l \cos \delta) \\ R_{12} &= \cos \psi_0 (-\sin \eta \sin \delta \sin \gamma + \sin l \cos \eta \sin \delta \cos \gamma + \cos \eta \cos l \cos \delta) \\ &\quad - \sin \psi_0 (\sin \eta \cos \gamma + \sin l \cos \eta \sin \gamma). \end{aligned}$$

Defining

$$\begin{aligned} f_+(t, \eta, \gamma, \delta, l) &= (\sin \eta \cos \gamma(t) + \sin l \cos \eta \sin \gamma(t))^2 \\ &\quad - (-\sin \eta \sin \delta \sin \gamma(t) + \sin l \cos \eta \sin \delta \cos \gamma(t) + \cos \eta \cos l \cos \delta)^2 \end{aligned} \quad (12)$$

and

$$\begin{aligned} f_\times(t, \eta, \gamma, \delta, l) &= 2 (\sin \eta \cos \gamma(t) + \sin l \cos \eta \sin \gamma(t)) \\ &\quad \times (-\sin \eta \sin \delta \sin \gamma(t) + \sin l \cos \eta \sin \delta \cos \gamma(t) + \cos \eta \cos l \cos \delta) \end{aligned} \quad (13)$$

we have

$$\begin{aligned} R_{11}^2 - R_{12}^2 &= \cos 2\psi_0 f_+(t) + \sin 2\psi_0 f_\times(t) \\ 2 R_{11} R_{12} &= \cos 2\psi_0 f_\times(t) - \sin 2\psi_0 f_+(t) \end{aligned}$$

and

$$h_{bar}(t) = [\cos 2\psi_0 f_+(t) + \sin 2\psi_0 f_\times(t)] h_+(t) + [\cos 2\psi_0 f_\times(t) - \sin 2\psi_0 f_+(t)] h_\times(t). \quad (14)$$

Using Eq. 7 and Eq. 14, the waveform is given by

$$\begin{aligned} h_{bar}(t) &= h_c (1 + \cos^2 i) [\cos 2\psi_0 f_+(t) + \sin 2\psi_0 f_\times(t)] \cos(\omega_0 t + \Phi(t) + \Phi_0) \\ &\quad + h_c (2 \cos i) [\cos 2\psi_0 f_\times(t) - \sin 2\psi_0 f_+(t)] \sin(\omega_0 t + \Phi(t) + \Phi_0). \end{aligned} \quad (15)$$

The reception patterns $f_+(t)$ and $f_\times(t)$ are shown in Fig. 2 for a signal from 47 Tuc. Writing the time-dependent sine and cosine terms in Eq. 15 as exponentials and defining

$$\begin{aligned} F_+(t) &= \exp[j\Phi(t)] f_+(t) \\ F_\times(t) &= \exp[j\Phi(t)] f_\times(t) \end{aligned} \quad (16)$$

the expression for the gravity wave strain along the bar axis is

$$\begin{aligned}
h_{bar}(t) = & \frac{1}{2}h_c (1 + \cos^2 i) \exp(j\Phi_0) [\cos 2\psi_0 F_+(t) + \sin 2\psi_0 F_\times(t)] \exp(j\omega_0 t) \\
& + \frac{1}{2}h_c (1 + \cos^2 i) \exp(-j\Phi_0) [\cos 2\psi_0 F_+^*(t) + \sin 2\psi_0 F_\times^*(t)] \exp(-j\omega_0 t) \\
& - \frac{j}{2}h_c (2 \cos i) \exp(j\Phi_0) [\cos 2\psi_0 F_\times(t) - \sin 2\psi_0 F_+(t)] \exp(j\omega_0 t) \\
& + \frac{j}{2}h_c (2 \cos i) \exp(-j\Phi_0) [\cos 2\psi_0 F_\times^*(t) - \sin 2\psi_0 F_+^*(t)] \exp(-j\omega_0 t).
\end{aligned} \tag{17}$$

We are now in position to calculate the anticipated signal as it would appear in the ALLEGRO data stream. This is most clearly presented in the frequency domain. Fourier transforming Eq. 9, the force produced on the bar is

$$\mathcal{F}(\omega) = -\frac{1}{2}\mu L_e \omega^2 h_{bar}(\omega). \tag{18}$$

This driving force produces motion of the transducer

$$H(\omega) = G(\omega) \mathcal{F}(\omega) = -\frac{1}{2}\mu L_e \omega^2 G(\omega) h_{bar}(\omega)$$

where $G(\omega)$ is the transfer function which relates transducer motion (or equivalently voltage) to the applied force [17]. We note that the overall calibration is contained in the transfer function. Defining a new transfer function (strain to transducer motion)

$$G_f(\omega) = -\frac{1}{2}\mu L_e \omega^2 G(\omega)$$

we write the signal as it appears in the data as simply

$$H(\omega) = G_f(\omega) h_{bar}(\omega) \tag{19}$$

with $h_{bar}(\omega)$ given by the Fourier transform of Eq. 17.

At this point in the signal chain, in the interest of limiting the bandwidth of sample data required, the signal is mixed with a reference (whose frequency is chosen to be between the two detection mode frequencies) and low-pass filtered using a commercial lock-in amplifier [4]. The lock-in provides both in-phase (x) and quadrature (y) outputs, so both amplitude and phase information is available on a bandwidth of 125 Hz containing the resonant modes of the detector. In software, the in-phase and quadrature components were combined to form a complex data stream

$$z(t) = x(t) + j y(t)$$

which was then demodulated to a 1 Hz bandwidth around each of the resonant modes [9]. We describe the complete demodulation from 1 kHz to 1 Hz, including both the hardware and software lockins, as mixing the signal with a single reference $\exp[j(\omega_r t + \phi_r)]$, where ω_r is the reference frequency and ϕ_r is an unknown reference phase (this phase can in fact be measured, but for the data set in question was not). Returning to the time domain for clarity the mixed signal is

$$H(t) = [G_f(t) \star h_{bar}(t)] \exp[j(\omega_r t + \phi_r)] \tag{20}$$

where ‘ \star ’ indicates a convolution. Using the expression from Eq. 17 we get

$$\begin{aligned}
H(t) = & G_f(t) \star \left(\frac{1}{2}h_c (1 + \cos^2 i) [\cos 2\psi_0 F_+^*(t) + \sin 2\psi_0 F_\times^*(t)] \exp[-j(\Phi_0 - \phi_r + (\omega_0 - \omega_r)t)] \right. \\
& \left. + \frac{j}{2}h_c (2 \cos i) [\cos 2\psi_0 F_\times^*(t) - \sin 2\psi_0 F_+^*(t)] \exp[-j(\Phi_0 - \phi_r + (\omega_0 - \omega_r)t)] \right).
\end{aligned} \tag{21}$$

Since ω_r is on the order of 1 kHz, the effect of the low-pass filtering is to remove terms from $H(t)$ which contain the sum frequencies ($\omega_r + \omega_0$). Now returning to the frequency domain, the signal, after demodulation, can be written

$$\begin{aligned}
H(\omega) = & \frac{1}{2}h_c (1 + \cos^2 i) \exp[-j(\Phi_0 - \phi_r)] G_f(\omega) [\cos 2\psi_0 F_+(\omega') + \sin 2\psi_0 F_\times(\omega')] \\
& - \frac{j}{2}h_c (2 \cos i) \exp[-j(\Phi_0 - \phi_r)] G_f(\omega) [\cos 2\psi_0 F_\times(\omega') - \sin 2\psi_0 F_+(\omega')]
\end{aligned} \tag{22}$$

where $\omega' = \omega \pm (\omega_0 - \omega_r)$ is the (positive or negative) downconverted signal frequency.

VI. DETECTION CONSIDERATIONS

Equation 22 gives the form of the CW signal as it would appear in the Allegro data. We now ask: “Is this signal in the data?” Since the strength of the signal is small compared to the detector noise (otherwise we would see it on a spectrum analyzer!), some work needs to be done to answer this question. We will use the standard maximum likelihood method to guide the analysis, but in the end the question of whether a signal was detected or not will be answered experimentally.

The likelihood function can be written

$$\Lambda = \frac{P(z|H)}{P(z|0)} \quad (23)$$

with $P(H|z)$ the probability that, given the observed data $z(t)$, the signal $H(t)$ is present, $P(z|H)$ the probability that, given the signal $H(t)$ is present, we observed the data $z(t)$, and $P(z|0)$ the probability that, given no signal present, we observe the data $z(t)$.

From [15], if

$$z = z_1, z_2, \dots, z_N$$

is the time-ordered sequence of detector output (in our case imaginary) and

$$H = H_1, H_2, \dots, H_N$$

is the signal waveform at the same sample times, then

$$P(z|0) = \frac{1}{[(4\pi)^N \det||R_{gh}||]} \exp\left(-\frac{1}{2} \sum_{g,h=0}^{N-1} R_{gh}^{-1} z_g z_h^*\right) \quad (24)$$

and

$$P(z|H) = \frac{1}{[(4\pi)^N \det||R_{gh}||]} \exp\left(-\frac{1}{2} \sum_{g,h=0}^{N-1} R_{gh}^{-1} (z_g - H_g)(z_h - H_h)^*\right) \quad (25)$$

where the R_{gh}^{-1} is the inverse of the autocorrelation matrix.

Substituting from above, the likelihood ratio is

$$\Lambda = \exp\left(-\frac{1}{2} \sum_{g,h=0}^{N-1} R_{gh}^{-1} (-z_g H_h^* - H_g z_h^* + H_g H_h)\right) \quad (26)$$

which, given the properties of the complex autocorrelation matrix [9], can be written

$$\Lambda = \exp\left(\Re\left\{\sum_{g,h=0}^{N-1} R_{gh}^{-1} z_g H_h^*\right\} - \frac{1}{2} \sum_{g,h=0}^{N-1} R_{gh}^{-1} H_g H_h^*\right) \quad (27)$$

where \Re means “take the real part”.

We define the following notation: x_k for the discrete Fourier transform of $x(t)$, evaluated at $\omega_k = 2\pi k/N\Delta t$, and $Sn_k^{(1)}$ is the one-sided PSD. Using the relation [16]

$$\sum_{g,h=0}^{N-1} R_{gh}^{-1} x_g x_h^* = 2\Delta f \sum_{k=0}^{N-1} \frac{x_k x_k^*}{Sn_k^{(1)}} \quad (28)$$

and taking the natural logarithm of the the likelihood function (to remove the exponential), we have

$$\ln \Lambda = 2\Delta f \Re\left\{\sum_{k=0}^{N-1} \frac{z_k H_k^*}{Sn_k^{(1)}}\right\} - \Delta f \sum_{k=0}^{N-1} \frac{|H_k|^2}{Sn_k^{(1)}}. \quad (29)$$

Substituting for H gives,

$$\begin{aligned}
\ln \Lambda &= 2\Delta f \Re \left(\exp[-j(\Phi_0 + \phi_r)] \sum_{k=0}^{N-1} \frac{z_k G_{f_k}^*}{S n_k^{(1)}} \right) \\
&\times \left[\frac{1}{2} h_c (1 + \cos^2 i) \cos 2\psi_0 F_{+k}^* + \frac{1}{2} h_c (1 + \cos^2 i) \sin 2\psi_0 F_{\times k}^* \right. \\
&- \left. \frac{j}{2} h_c (2 \cos i) \cos 2\psi_0 F_{\times k}^* + \frac{j}{2} h_c (2 \cos i) \sin 2\psi_0 F_{+k}^* \right] \\
&- \Delta f \sum_{k=0}^{N-1} \frac{1}{S n_k^{(1)}} \\
&\times \left[\frac{1}{4} h_c^2 (1 + \cos^2 i)^2 \cos^2 2\psi_0 |G_{f_k} F_{+k}|^2 + \frac{1}{4} h_c^2 (1 + \cos^2 i)^2 \sin^2 2\psi_0 |G_{f_k} F_{\times k}|^2 \right. \\
&+ \left. \frac{1}{4} h_c^2 (2 \cos i)^2 \cos^2 2\psi_0 |G_{f_k} F_{\times k}|^2 + \frac{1}{4} h_c^2 (2 \cos i)^2 \sin^2 2\psi_0 |G_{f_k} F_{+k}|^2 \right]
\end{aligned} \tag{30}$$

where terms of the form

$$\sum_{k=0}^{N-1} F_{+k} F_{\times k}^*$$

sum to zero.

To simplify the notation of Eq. 30, we make the following definitions:

$$\begin{aligned}
q_+ &= \Delta f \sum_{k=0}^{N-1} \frac{z_k G_{f_k}^* F_{+k}^*}{S n_k^{(1)}} \\
q_\times &= \Delta f \sum_{k=0}^{N-1} \frac{z_k G_{f_k}^* F_{\times k}^*}{S n_k^{(1)}} \\
\rho_+ &= \Delta f \sum_{k=0}^{N-1} \frac{|G_{f_k} F_{+k}|^2}{S n_k^{(1)}} \\
\rho_\times &= \Delta f \sum_{k=0}^{N-1} \frac{|G_{f_k} F_{\times k}|^2}{S n_k^{(1)}} \\
a_1 &= h_c (1 + \cos^2 i) \cos 2\psi_0 \\
a_2 &= h_c (1 + \cos^2 i) \sin 2\psi_0 \\
a_3 &= h_c (2 \cos i) \cos 2\psi_0 \\
a_4 &= h_c (2 \cos i) \sin 2\psi_0.
\end{aligned} \tag{31}$$

The four quantities $\{q_+, q_\times, \rho_+, \rho_\times\}$ are familiar from signal processing theory. The first two, $\{q_+, q_\times\}$, are the outputs from applying independent optimal filters in the frequency domain for the two polarizations of the gravity wave. The second pair, $\{\rho_+, \rho_\times\}$ are the signal to noise ratios (energy) for the two polarizations. These four terms are completely specified, up to the unknown signal frequency. The four a_i 's are the ‘‘amplitudes’’ containing the desired astrophysical information.

Substituting these into the likelihood function,

$$\begin{aligned}
\ln \Lambda &= a_1 \Re \{ \exp[j(\Phi_0 - \phi_r)] q_+ \} + a_2 \Re \{ \exp[j(\Phi_0 - \phi_r)] q_\times \} \\
&- a_3 \Re \{ j \exp[j(\Phi_0 - \phi_r)] q_\times \} + a_4 \Re \{ j \exp[j(\Phi_0 - \phi_r)] q_+ \} \\
&- \frac{1}{4} (a_1^2 \rho_+ + a_2^2 \rho_\times + a_3^2 \rho_\times + a_4^2 \rho_+).
\end{aligned}$$

We maximize the likelihood function over the a_i 's which yields the following four expressions:

$$a_1 = 2 \frac{|q_+|}{\rho_+} \cos(\Phi_0 - \phi_r + \phi_+) \tag{32}$$

$$\begin{aligned}
a_2 &= 2 \frac{|q_\times|}{\rho_\times} \cos(\Phi_0 - \phi_r + \phi_\times) \\
a_3 &= -2 \frac{|q_\times|}{\rho_\times} \sin(\Phi_0 - \phi_r + \phi_\times) \\
a_4 &= 2 \frac{|q_+|}{\rho_+} \sin(\Phi_0 + \phi_r - \phi_+)
\end{aligned}$$

where the filtered outputs have been expressed as

$$q_{(+,\times)} = |q_{(+,\times)}| \exp(j\phi_{(+,\times)})$$

with $\phi_{(+,\times)} = \arg[q_{(+,\times)}]$. Finally,

$$\sum_{i=1}^4 a_i^2 = 4 \left(\frac{|q_+|^2}{\rho_+^2} + \frac{|q_\times|^2}{\rho_\times^2} \right) = h_c^2 [(1 + \cos^2 i)^2 + 4 \cos^2 i] = \langle h_+^2 + h_\times^2 \rangle \quad (33)$$

which, to factors, is the energy of the gravitational wave. Note that this depends on the unknown signal frequency f_0 . As described below, we will assume values for the gravitational wave frequency, and use that to calculate Eq. 33. The end result of the analysis is a “spectrum” of energy at a given signal frequency. We shall report this as a “strain amplitude”, given by the square root of Eq. 33

$$h_s(f_0) = \sqrt{h_+^2(f_0) + h_\times^2(f_0)}.$$

VII. EXPERIMENTAL CONSIDERATIONS

Calculation of Eq. 33 involved a number of steps. First, the archived data was read off tape and narrowbanded to a 1 Hz bandwidth around each of the resonant modes [9] where ALLEGRO is most sensitive. This was done to reduce the computational requirements. Next, the mode amplitudes were “cleaned” of large, transient events (section VII A). Finally, the cleaned data was discrete Fourier transformed and optimal filters were applied (section VII B).

A. data selection

Even with ALLEGRO’s high duty cycle, there were periods of missing or unusable data. Data losses came in basically three flavors. (1) Transient electronic effects which lasted on the order of a second. (2) Longer periods when the detector was undergoing some form of maintenance. (3) The clock losing phase lock to WWVB. The transient disturbances were the most frequent, occurring at a rate of one or two per day. They usually involved a sudden change in the flux threading the SQUID loop (hence the name “flux jumps”). The majority of the flux jumps occurred when the dc level of the SQUID reached a pre-determined maximum (5 volts). The electronics controlling the SQUID then reset the dc voltage to zero, causing a short and violent jump in the in-phase and quadrature channels of the data, as shown in Fig. 3.

Frequently electronic interference reaching the SQUID caused flux jumps. In the past when data tapes were erased (the degaussing takes place in a separate room from the main experiment), the end of the degaussing cycle produced a noise spike which traveled through the wiring in the wall, through the computers, and from there to the SQUID. Once recognized, an isolating transformer was placed between the degausser and the wall socket, fixing the problem. Another common type of transient signal is a “spike”. These look similar to flux jumps in the data and there is some suspicion that they are in fact flux jumps, but essentially they are of unknown origin. All of these noisy periods were short enough so that the affected data could be removed and the resulting gap interpolated across. This was done using the MATLAB *interp1* routine. Interpolation was performed on the resampled data. It was usual to interpolate across 1-5 seconds of data, using the 10-20 seconds of data before and after the gap for the interpolation template.

For longer sections of unusable data or for periods of missing data, the analysis was stopped and restarted after the disturbance. By “restarted” we mean that the accumulation of data was stopped, the accumulated data purged, and the analysis started up again on the data immediately following the disturbance. The most common cause of data loss was transferring liquid helium into the dewar which removed a couple of hours of data every week. Another cause of long stretches of unusable data were large excitations of the resonant modes due to earthquakes around the

globe. Earthquakes were identified by a unique signature in the low frequency housekeeping channel. It was usual for an earthquake to produce multiple large excitations over a few tens of minutes, often resulting in saturation of the A/D's. Computer down time, calibration of the detector and other maintenance all caused gaps in the data, although infrequently.

The final type of data loss was associated with the WWVB clock. Frequently when the weather between Baton Rouge and NIST at Boulder, Colorado was bad, the clock we used to control the sampling of the data lost phase lock to the WWVB radio signal. When this happened, the clock's internal oscillator "freewheeled" with the result that the time between samples was no longer consistently 8 ms. Deviations in the sampling rate from 8 ms were called "timing jumps". A jump in the time between when samples were taken produced a corresponding jump in the phase of modes and the calibrator signal as shown in Fig. 4. The most frequent jumps were on the order of 1-2 ms, producing a phase jump in a sinusoidal signal at the mode frequencies of approximately 1/100 of a cycle. This was considered an acceptable level of uncertainty in the ability to track the phase of a potential gravity wave signal. These small jumps were noted but ignored. Larger jumps produced correspondingly larger jumps in phase and were considered unacceptable. When they occurred, the analysis was stopped at the timing jump and restarted again after the glitch. The frequency and size of the timing jumps were highly variable. During the winter of 1994 the smaller jumps occurred almost once per day while the larger jumps rarely happened. By the spring of that year, the trend was reversed and much data was lost due to the inconsistency of the clock.

B. the filters

The ability of our analysis filters to match the phase of the gravity wave determined the amount of continuous data which could be analyzed at one time. We refer to this as a "record". Ideally, the length of a record would be set by the available computational facilities. This was not the case. Instead, the record length was limited by our electronics. The function generator which supplied the reference frequency to the lock-in detector had some drift associated with it. This drift limits the ability of the filter to match the phase of the gravity wave signal in the data. Careful measurements of the drift led to the conservative conclusion that roughly 28 hours (10^5 sec) was the longest period of time for which we could expect the filter to remain in phase with the signal [9]. The less conservative conclusion was roughly three times longer, but we prefer to be cautious with the analysis. The reference signal to the lock-in has since been phase locked to GPS, greatly improving the phase stability. Given the above considerations, there were 34 records available from days 1-94 of 1994, for a total of 944.44 hours of data.

Performing a discrete Fourier transform on 10^5 sec worth of data results in a frequency resolution of the search of 10^{-5} Hz. The optimal filters also depend on the signal frequency. With no known source available, we assume there is a potential signal every 10 μ Hz in the ranges 896.30-897.30 Hz and 919.76-920.76 Hz. Each assumed signal frequency was used in turn to create the F_+ and F_\times components of the signal template.

The other two components of the filters, the bar transfer function and the power spectral density, depend on the resonant frequency and damping time of the coupled bar-transducer system. As both quantities experienced slow drifts due to, for example, temperature changes in the dewar, it was necessary to measure them for each record (see Fig. 5 and Fig. 6 respectively). For each mode, a low variance power spectral density was formed from the cleaned data. A Lorentzian curve was then fit to each PSD using the MATLAB *curvefit* routine, which finds the best fit to a function in the least-squares sense. The Lorentzian was characterized by four parameters: the white-noise level (S_0), the peak height (S_1), the frequency of the resonance (ω_\pm), and the width (or the damping time - τ_\pm). The resulting fitted parameters for each record were then stored on disk to be retrieved as necessary. The power spectral density component of the optimal filter was calculated for a record by

$$Sn(\omega_k) = S_0 + \frac{(S_1 - S_0)}{\tau_\pm^2} [(\omega_k^2 - \omega_\pm^2)^2 + \omega_k^2/\tau_\pm^2]^{-1}. \quad (34)$$

Similarly, the bar transfer function was calculated from the functional

$$G(\omega_k) = k_\pm \frac{\omega_\pm}{\tau_\pm} [\omega_\pm^2 + j\omega_k/\tau_\pm - \omega_k^2]^{-1} \quad (35)$$

where the parameters are those given above. The constant k_\pm sets the calibration for each mode [17].

C. computational reduction

Even though this search was directed towards only a small section of the sky, it was still cpu intensive on the available computing facilities. Applying 2×10^5 different filters, where each new set of filter coefficients required a Fourier transform on a time sequence of 10^5 elements, was prohibitively time consuming.

The signal frequency enters into calculation of the filter coefficients in two places; through the carrier wave and in the Doppler shift. However, as the phase modulation is slowly varying with respect to the carrier wave, it was not necessary to re-calculate the phase correction due to the Doppler shift for each assumed signal frequency. Instead, the Doppler shift was calculated at specific choices of the signal frequency, which were then used to approximate signal templates over a range of frequencies.

The maximum fractional frequency shift of a signal from the two sources over the course of a year is

$$\frac{|\delta f(f_0)|}{f_0} \sim \begin{cases} 5 \times 10^{-5} & 47 \text{ Tuc} \\ 10^{-4} & \text{galactic center} \end{cases}$$

at the signal frequencies of interest. To approximate all phase shifts in a range of signal frequencies $f_0 \pm \Delta f_0$ with a calculation at a single signal frequency, then the error made must be less than the frequency resolution of the search. Defining the error as

$$\delta f(f_0 \pm \Delta f_0) - \delta f(f_0) = 5 \times 10^{-5} \Delta f_0$$

we have the maximum range of signal frequencies over which the approximation is valid is given by

$$|\Delta f_0| \leq \begin{cases} 0.2 \text{ Hz, } 47 \text{ Tuc} \\ 0.1 \text{ Hz, galactic center} \end{cases}$$

Using this information, we calculated independent F_+ , F_\times components of the signal template at the frequencies 896.45 Hz, 896.80 Hz, 897.15 Hz, 919.91 Hz, 920.26 Hz and 920.61 Hz for the 47 Tuc analysis. For the galactic center analysis, signal templates were calculated every 0.2 Hz in the range 896.40 Hz - 897.20 Hz for the minus mode, and 919.86 Hz - 920.66 Hz for the plus mode.

VIII. RESULTS

The real and imaginary components of the data stream, in the absence of a signal, are zero mean Gaussian distributed. Neither the Fourier transform or the filtering changes the underlying distribution and therefore the real and imaginary parts of the filtered outputs $q_{(+,\times)}$ are also individually zero mean Gaussian distributed. Given this, calculation of Eq. 33 at a particular choice of the signal frequency, taken from a particular data record, results in a sample drawn from a chi-squared distribution with four degrees of freedom [18]. If the signal is absent, this is given by

$$p(E) = \frac{1}{(2\sigma^2)^2} E \exp(-E/2\sigma^2). \quad (36)$$

where $E = h_s^2(f_0)$.

The total number of available data records provide an ensemble of experiments each making 2×10^5 measures of E at the assumed values for f_0 . Since the signal is expected to be long-lived, much longer than the operational time of the detector, we improve our estimate of the energy by taking the ensemble average of the individual measures:

$$\bar{E} = \frac{1}{N} \sum_{i=1}^N E_i \quad (37)$$

where $N = 34$ is the number of available data records. We calculate the strain amplitude $h_s(f_0)$ by taking the square root of \bar{E} . As each ensemble is generated by the sum of four terms (Eq. 33) and there are 34 data records averaged together, from the central limit theorem we can accurately describe the distribution of $h_s(f_0)$ as gaussian.

The resulting ‘‘spectra’’ of $h_s(f_0)$ vs. f_0 are shown in Fig. 7 for 47 Tuc and Fig. 8 for the galactic center analysis. It is important to remember that the abscissa is not a Fourier frequency but rather the assumed frequency of the gravitational wave. That the plus mode shows a lower strain value than the minus mode reflects the fact that the

plus mode has a higher quality factor and is therefore more sensitive. That the results of the galactic center analysis seem somewhat “shifted” with respect to the 47 Tuc results is due to the effects of the Doppler shifts. For a signal from 47 Tuc during the period over which data was analyzed, a signal at a particular frequency, for example 920 Hz, experienced periods of both red shift and blue shift. On average, therefore, the signal was experiencing detector noise at roughly 920 Hz. For the galactic center analysis, during this period an incoming signal was experiencing maximum blue-shift, and was never red-shifted. Therefore, a signal at 920 Hz would be experiencing detector noise at a slightly higher frequency, resulting in a graph that seems “a bit skewed to the right” with respect to the 47 Tuc analysis.

The question still remains if there is a real signal at a particular frequency. It is unlikely that the detector is dominated by CW radiation. We expect the number of real signals which would be extracted by our analysis to be small with respect to the number of possible signals (i.e. the number of frequencies at which we assume there to be a signal). We can therefore answer the question experimentally. We normalize $h_s(f_0)$ at each f_0 to its mean value. This new variable has a distribution independent of the detector noise at each signal frequency.

The histograms of the resulting normalized spectra are shown in Fig. 9 for 47 Tuc and Fig. 10 for the galactic center analysis. Given our reasonable assumption that the detector is not wave-dominated, the majority of the normalized measures form an experimental estimation of the parent distribution for the detector noise from which each individual measure is drawn. If the strain amplitude at a particular signal frequency lies outside this distribution, it is identified as a candidate for a real signal.

IX. DISCUSSION

Neither Fig. 9 or Fig. 10 shows any evidence for “outliers” which would suggest the possibility of having observed gravitational radiation from pulsar spin-down. The existence of burst-like non-gaussian noise in resonant bar data is well known, and this noise must be dealt with in any search for burst-like signals of gravitational waves. The encouraging result of this analysis is that for CW signals there is not a serious problem with non-gaussian noise in the resonant bar data. Thus, at least at the level of the current work, all the noise sources are well understood and the overall sensitivity may be improved in the future simply by increasing the length of the data record. We note that care was taken to use only data when the detector was operating well and procedures were implemented to smooth out other non-stationary effects. Astrophysically, at this level of sensitivity, the actual spin-down rate of a pulsar due to the energy lost as gravitational radiation would be large enough that the signal and its filter template would go out of phase by half a cycle after of order 5000 s, much less than the length of one record. This effect can be taken into account by including one or more spin-down parameters in the signal template, at the cost of significantly increasing the computational time of the search. Since there was no known source for ALLEGRO and somewhat limited computing resources available, we have essentially made a demonstration of the capabilities of resonant detectors for this type of search.

However, it is important to note that even with these restrictions, the analysis has reached a level of sensitivity which is astrophysically interesting. If a source were to become known with the correct frequency, and, as our sensitivity was limited by hardware which has been substantially improved, it seems likely that such a signal could be detected and new astrophysics learned.

X. CONCLUSION

We have searched for sources of continuous gravitational radiation from the globular cluster 47 Tuc and the galactic center at signal frequencies near 1 kHz using data taken by the ALLEGRO gravitational radiation detector in the first three months of 1994. No candidate signals were found, and a constraint of 8×10^{-24} was put on gravitational radiation emitted from pulsar spin-down at both locations.

ACKNOWLEDGMENTS

The authors thank Sam Finn and Joel Tohline for many helpful discussions. Much of the analysis and the final writing of this paper was done at the INFN Laboratori Nazionali di Frascati. E.M. thanks G. Pizzella, E. Coccia, and the ROG collaboration for their support. The LSU group was supported by the National Science Foundation under Grant No. PHY-9311731.

- [1] K. C. B. New et al. *ApJ*, 450, 757-763, 1995
- [2] Benjamin J. Owen et al. *Phys. Rev. D*, 58, 084020-084034, 1998
- [3] S. L. Shapiro and S. A. Teukolsky. *Black Holes, White Dwarfs and Neutron Stars*. Wiley, New York, 1983.
- [4] E. Mauceli et al. *Phys. Rev. D*, 54, 1264-1275 (1996).
- [5] P. Astone, S. Frasca, G. V. Pallottino, and G. Pizzella, in *Proceedings of the 12th Italian Conference on General Relativity and Gravitation, Rome, September 1996*, edited by M. Bassan, I. Modena, V. Ferrari, and M. Francaviglia (World Scientific Publishing Co., Singapore, 1997).
- [6] J. H. Taylor et al. Catalog of 706 pulsars (1995 update). *ApJS*, 88, 529, 1993.
- [7] Bernard F. Schutz and M. Alessandra Papa in *Proceedings of the January 1999 Moriond meeting on Gravitational Waves and Experimental Gravity* (gr-qc/9905018)
- [8] R. N. Manchester et al. *Nature*, 352, 18 July (1991).
- [9] E. Mauceli. Ph.D. Dissertation. Louisiana State University (1997).
- [10] P. R. Brady et al. *Phys. Rev. D*, 57, 2101 (1998).
- [11] C. Misner, K. Thorne, and J. A. Wheeler. *Gravitation* W. H. Freeman and Co., San Francisco.
- [12] D.V. Gal'tsov, V.P. Tsvetkov, and A.N. Tsirulev *Sov. Phys. JETP* 59, 472 (1984)
- [13] M. Zimmermann and E. Szedenits, Jr. *Phys. Rev. D*, 20, 351 (1979).
- [14] H. Goldstein. *Classical Mechanics*. Addison-Wesley, Massachusetts, 1980.
- [15] L. A. Wainstein and V. D. Zubakov. *Extraction of Signals from Noise*. Dover Press, New York, 1962.
- [16] S. Finn. *Phys. Rev. D*, 46, 5236-5249 (1992).
- [17] A. Morse, W.O. Hamilton, W. W. Johnson, E. Mauceli and M. P. Mchugh. *Phys. Rev. D*, 59, 062002 (1999).
- [18] A. D. Whalen. *Detection of Signals in Noise*. Academic Press, New York and London, 1971.

FIG. 1. Frequency shift of a signal from 47 Tuc arriving at the ALLEGRO detector on January 1-2, 1994.

FIG. 2. The reception patterns for the plus polarization (solid line) and the cross polarization (dot-dashed line) of a signal from 47 Tuc.

FIG. 3. A SQUID reset in the in-phase and quadrature channels of the data stream.

FIG. 4. A 1 ms jump in the sampling time as it appears in the continuous system test signal (CST-a sinusoidal driving force applied to the bar at 865 Hz) [4].

FIG. 5. The measured resonant frequencies for each mode and each data record. The frequency is given as a shift relative to the measured frequency for the first data record.

FIG. 6. The measured damping times for each mode and each record.

FIG. 7. The strain amplitude of a gravitational wave from 47 Tuc at each assumed signal frequency near the plus and minus resonant modes. The lower values of the strains of the plus modes relative to the minus mode are due to the higher mechanical Q of the plus mode.

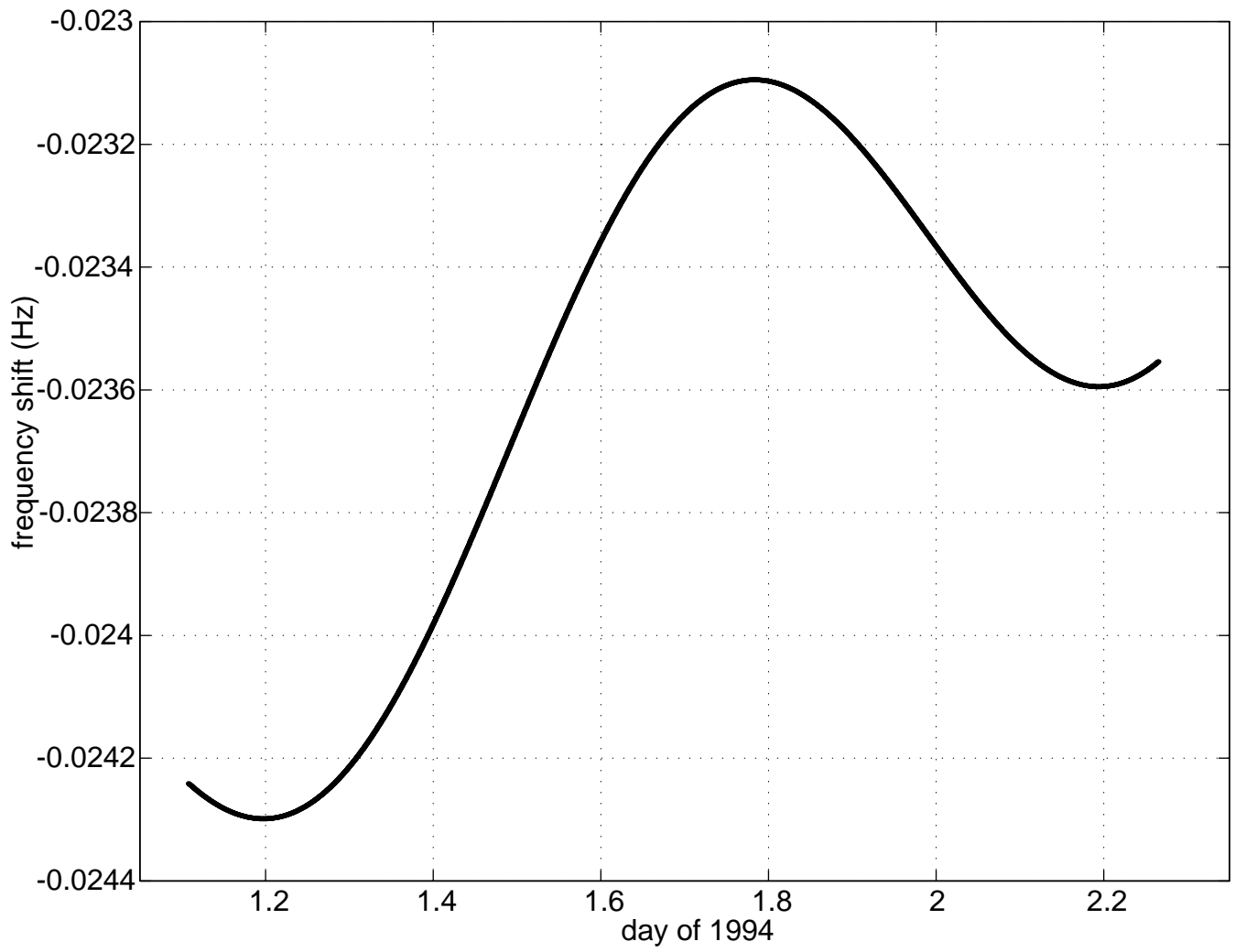
FIG. 8. The strain amplitude of a gravitational wave from the galactic center at each assumed signal frequency near the plus and minus resonant modes.

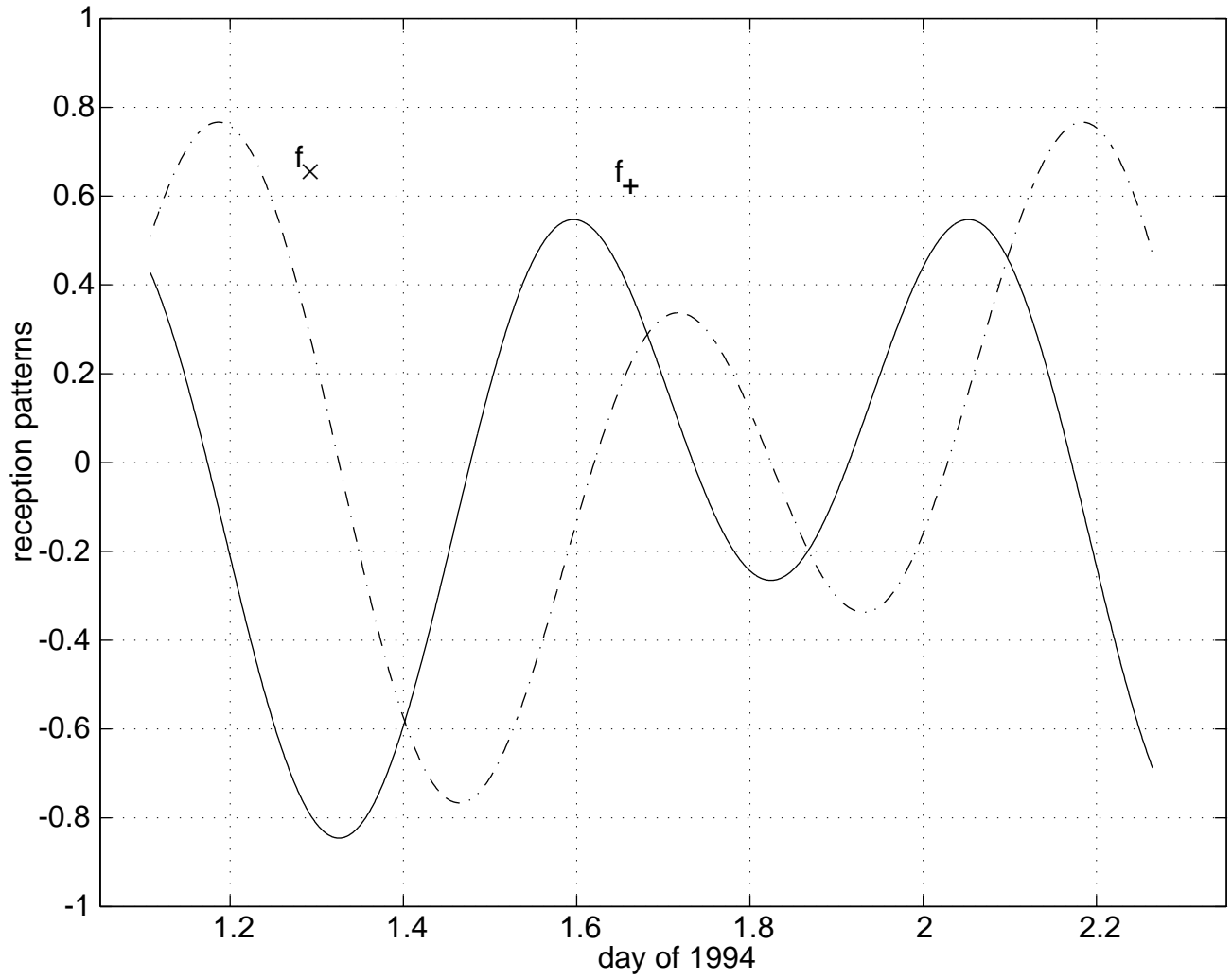
FIG. 9. Histograms of the normalized "spectrum" for signals from 47 Tuc near the minus and plus modes. The solid curve is a gaussian distribution with mean of one and variance derived from the normalized spectrum.

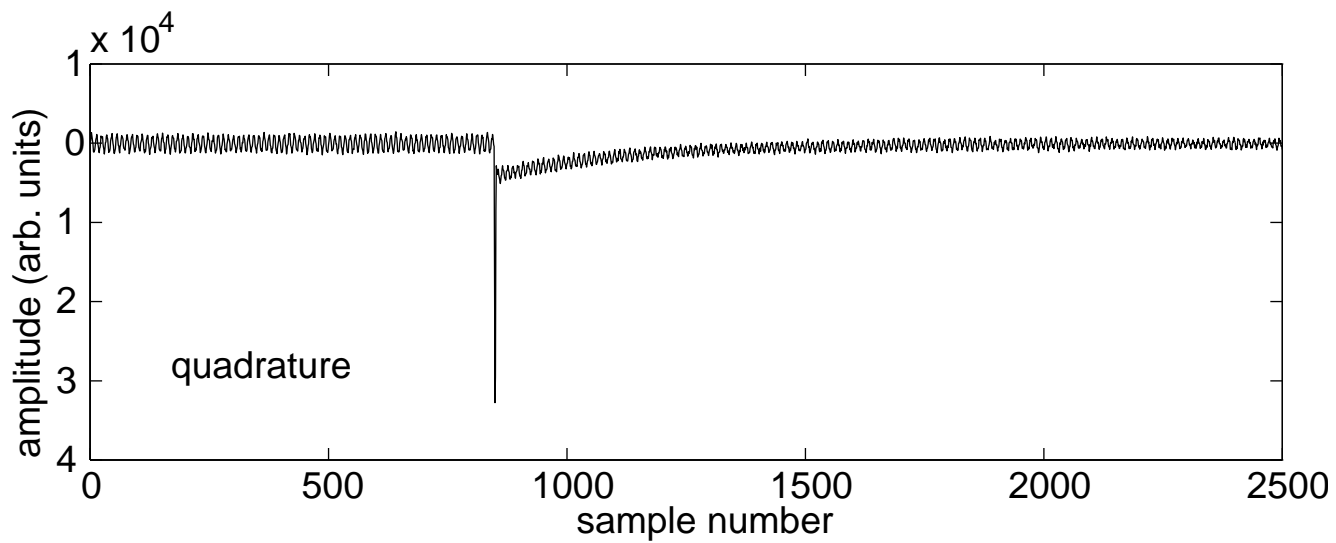
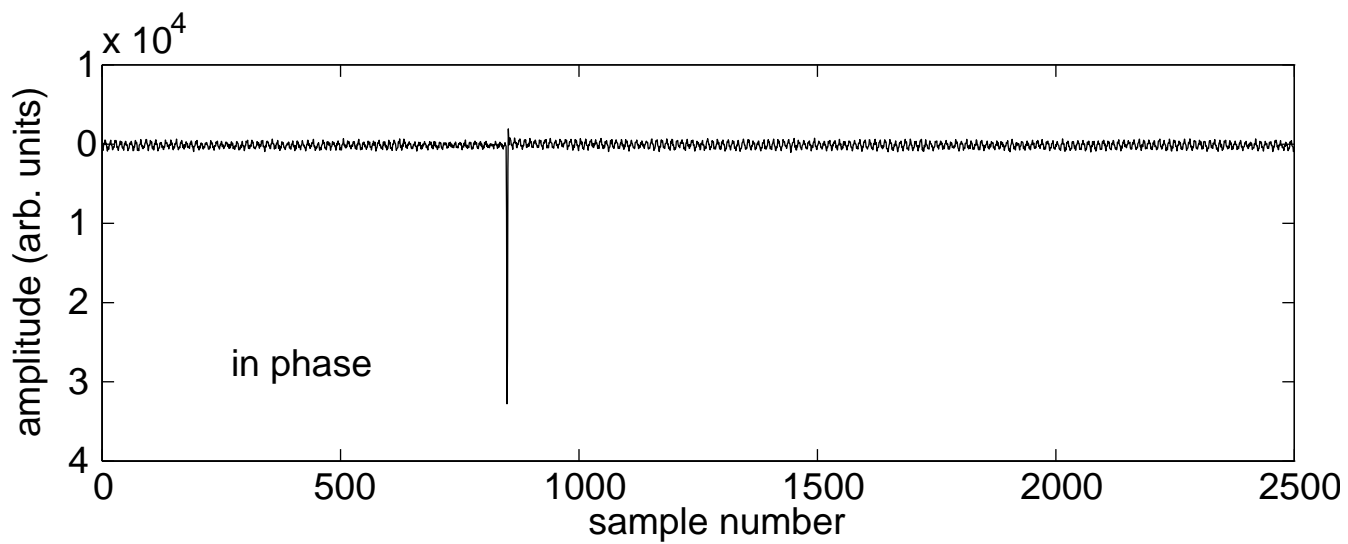
FIG. 10. Histograms of the normalized "spectrum" for signals from the galactic center near the minus and plus modes. The solid curve is a gaussian distribution with mean of one and variance derived from the normalized spectrum.

TABLE I. Coordinates for the two source locations

Source	RA (hrs:mins:secs)	declination (degs:mins:secs)	distance (kpc)
galactic center	17:42:29.3	-28:59:18	8.0
47 Tuc	00:24:06	-72:04:00	4.5

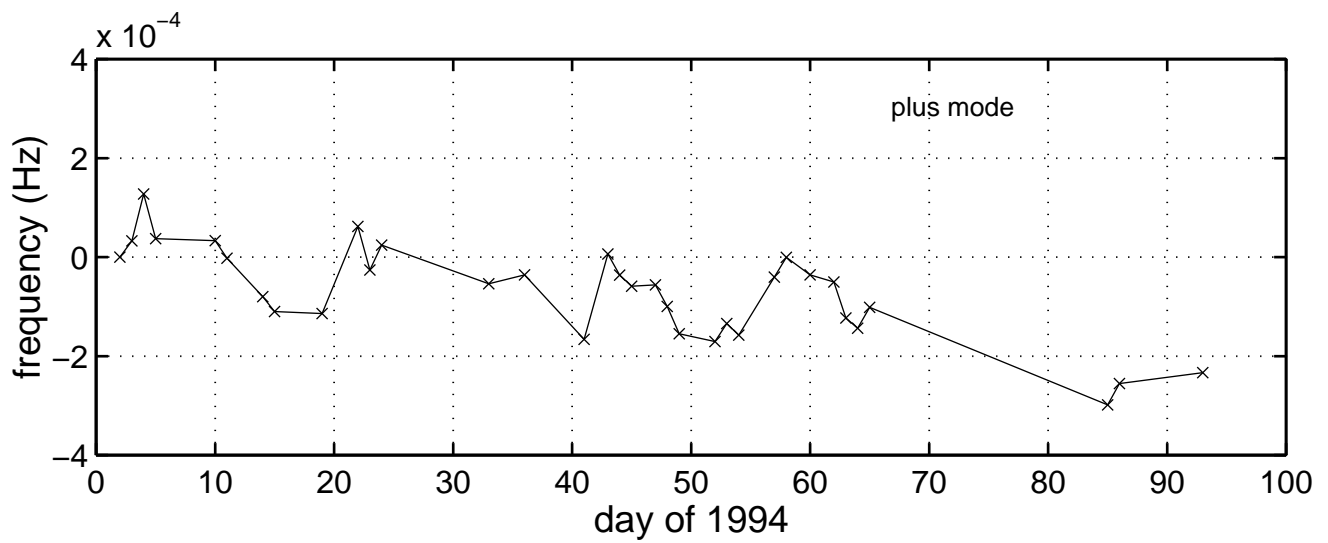
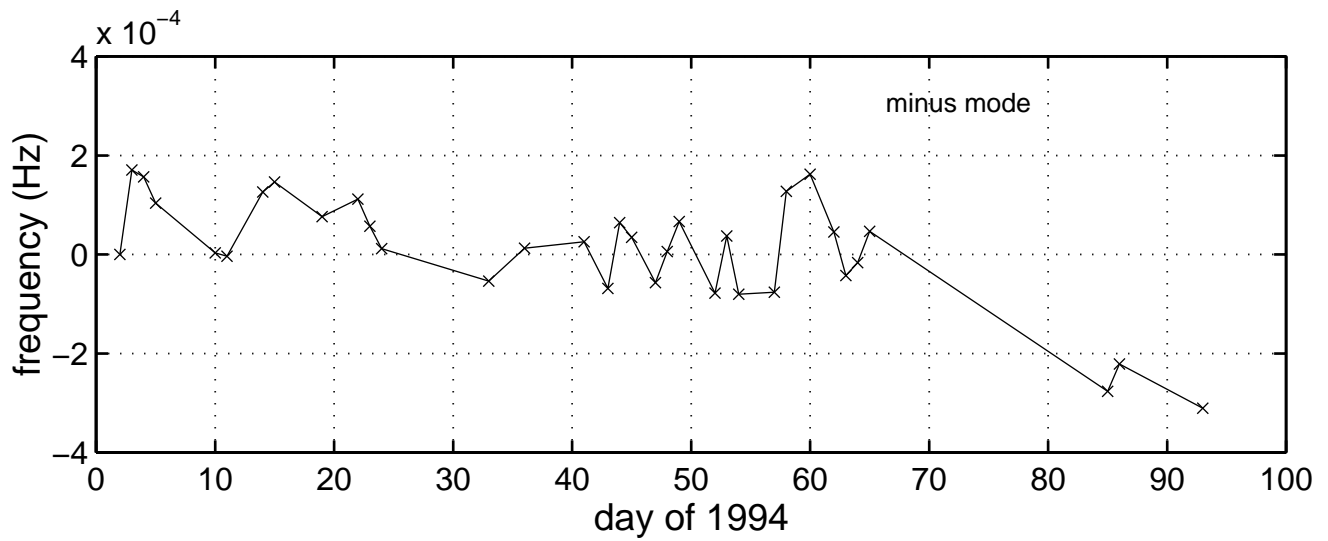


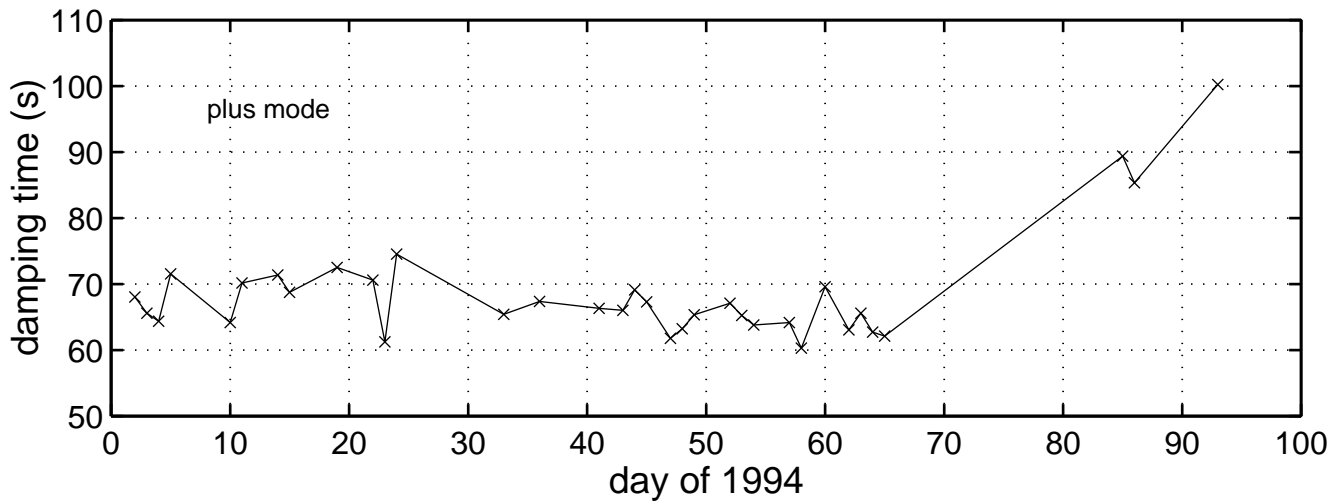
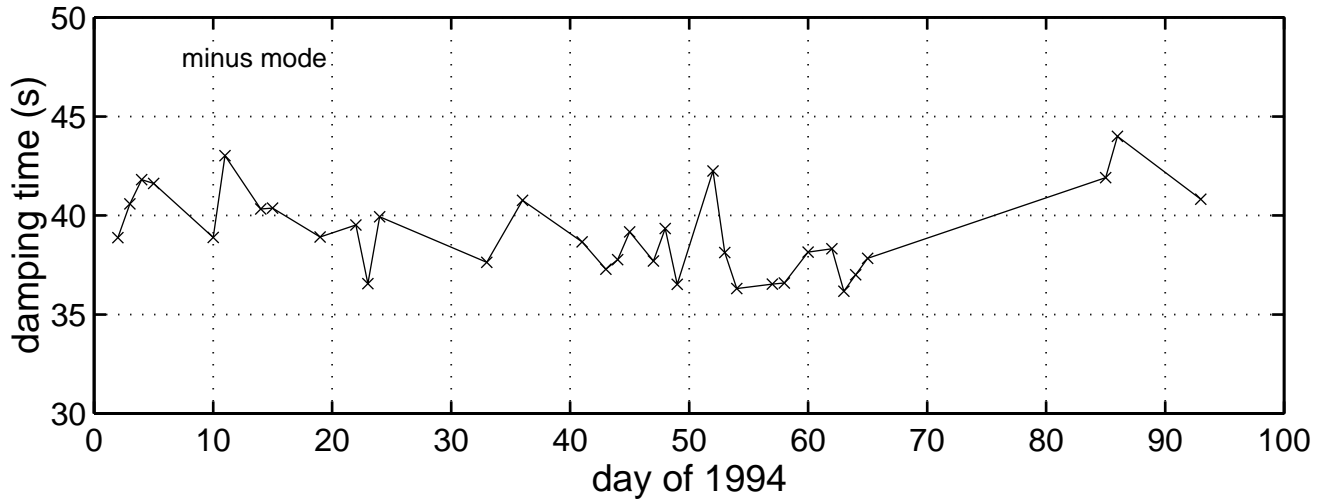




This figure "figure4.gif" is available in "gif" format from:

<http://arxiv.org/ps/gr-qc/0007023v1>





This figure "figure7.gif" is available in "gif" format from:

<http://arxiv.org/ps/gr-qc/0007023v1>

This figure "figure8.gif" is available in "gif" format from:

<http://arxiv.org/ps/gr-qc/0007023v1>

